# Nature of the Visual Loss in Observers With Leber's Congenital Amaurosis Caused by Specific Mutations in *RPE65*

Caterina Ripamonti,[1] G. Bruce Henning,[1] Robin R. Ali,[1] James W. Bainbridge,[1] Scott J. Robbie,[1] Venki Sundaram,[1] Vy A. Luong,[1] L. Ingeborgh van den Born,[2] Ingele Casteels,[3] Thomy J. L. de Ravel,[4] Anthony T. Moore,[1] and Andrew Stockman[1]

[1]UCL Institute of Ophthalmology, University College London, London, England
[2]Rotterdam Eye Hospital, Rotterdam, The Netherlands
[3]Department of Ophthalmology, University Hospitals Leuven, Leuven, Belgium
[4]Centre for Human Genetics, University Hospitals Leuven, Belgium

Correspondence: Andrew Stockman, UCL Institute of Ophthalmology, University College London, 11-43 Bath Street, London EC1V 9EL, England;
a.stockman@ucl.ac.uk.

**PURPOSE.** To characterize visual losses associated with genetic mutations in the *RPE65* gene that cause defects in the RPE-specific isomerase, RPE65. RPE65 is an important component of the retinoid cycle that restores 11-*cis*-retinal after its photoisomerization to its all-*trans* form. The defects investigated here cause Leber's congenital amaurosis (LCA2), an autosomal, recessively-inherited, severe, congenital-onset rod–cone dystrophy.

**METHODS.** Vision was assessed in nine patients and 10 normal controls by measuring: (1) long-wavelength sensitive (L-) cone temporal acuity (critical flicker fusion frequency or cff) as a function of target illuminance, and (2) L-cone temporal contrast sensitivity as a function of temporal frequency at a fixed-target illuminance. Measurements were made by modulating either a 650-nm light superimposed on a 480-nm background or the red phosphor of a color monitor on a background produced by the monitor's blue phosphor.

**RESULTS.** *RPE65*-mutant observers have severely reduced cffs with shallower cff versus log illuminance functions that rise with a mean slope of 4.53 Hz per decade of illuminance compared with 8.69 Hz in normal controls. Consistent with the cff differences, *RPE65*-mutant observers show losses in temporal contrast sensitivity that increase rapidly with temporal frequency.

**CONCLUSIONS.** All *RPE65*-mutant observers have consistent and substantial losses in temporal acuity and sensitivity compared with normal observers. The losses can be characterized by the addition of two sluggish filters within the mutant visual pathway, both filters with a time constant of 29.5 ms (i.e., low-pass filters with cut-off frequencies of 5.40 Hz).

Keywords: RPE65, rods and cones, scotopic, flicker sensitivity, temporal processing, LCA2, Leber's congenital amaurosis.

Leber's congenital amaurosis (LCA) is a group of severe, autosomal recessively inherited, congenital-onset rod–cone dystrophies that typically result in complete loss of vision in the third or fourth decade of life.[1,2] One form of the disease, LCA2, can be caused by more than 87 different mutations in the gene that encodes RPE65, an RPE-specific 65-kDa isomerase[3–8] (in the public domain, see, http://www.hgmd.org). Other mutations of the *RPE65* gene have been associated with recessive retinitis pigmentosa (RP20),[3,9] fundus albipunctatus,[10] and an autosomal dominant form of RP with choroidal involvement.[11] RPE65 catalyzes the isomerization of all-*trans*-retinyl esters to 11-*cis*-vitamin A. It is thus a key component of the visual cycle, the biochemical pathway that regenerates visual pigment after exposure to light.[12–18] Lack of functional RPE65 results in deficiency of 11-*cis* retinal, the light-sensitive chromophore that binds to the G protein–coupled receptor protein opsin, with the result that rod photoreceptor cells are unable to respond to light.[19,20] Therefore, LCA2 patients are usually night blind. By contrast, cone photoreceptors have access to 11-*cis* retinal

through an alternative pathway that does not depend on RPE65, thus allowing cone-mediated vision in younger patients with LCA2.[21,22]

Retinitis pigmentosa, of which LCA2 is one congenital form, is made up of a highly heterogeneous group of retinal degenerative hereditary diseases now known to be caused by mutations in more than 50 different genes.[23,24] Consequently, earlier psychophysical work on RP without genetic information is now of relatively limited use. The power of temporal acuity and temporal contrast-sensitivity measurements in the modern context of molecularly-characterized visual disorders is that the analysis and modelling of the functional loss can be directed at the specific molecular loss and its consequences.

Here, we consider the nature of the visual loss in a cohort of individuals with mutations in the gene encoding the RPE65 protein that cause LCA2; the mutations are specified in Table 1. In both affected individuals and normal observers we measured: (1) temporal acuity (sometimes called critical flicker fusion frequency or cff) as a function of target radiance, and (2)

TABLE 1. The Subject Codes, Sex, Age at Treatment, Genetic Mutation, and the Left and Right Eye Spatial Acuity at Time of Treatment (in logMAR)

| Subject Code | Sex | Age at Treatment, y, mo | Mutation | Left Eye Acuity, logMAR | Right Eye Acuity, logMAR |
|---|---|---|---|---|---|
| S1 | M | 24, 4 | Homozygous: c.[1102T>C] + [1102T>C] p.[Tyr368His] + [Tyr368His] | 1.16 | 0.88 |
| S3 | M | 18, 0 | Heterozygous: c.[16G>T] + [499G>T] p.[Glu6X] + [Asp167Tyr] | 0.50 | 0.76 |
| S5 | M | 23, 3 | Homozygous: c.[1102T>C] + [1102T>C] p.[Tyr368His] + [Tyr368His] | 0.31 | 0.36 |
| S6 | M | 17, 10 | Homozygous: c.[1102T>C] + [1102T>C] p.[Tyr368His] + [Tyr368His] | 0.53 | 0.68 |
| S7 | F | 10, 2 | Heterozygous: c.[11+5G>A] + [12-2A>G] p.[?] + [?] | 0.46 | 0.44 |
| S8 | M | 10, 5 | Homozygous: c.[271C>T] + [271C>T] p.[Arg91Trp] + [Arg91Trp] | 0.69 | 0.64 |
| S10 | M | 6, 2 | Heterozygous: c.[11+5G>A] + [1102T>C] p.[?] + [Tyr368His] | 0.80 | 0.70 |
| S11 | M | 13, 3 | Heterozygous: c.[370C>T] + [1590delC] p.[Arg124X] + [Phe530fs] | 0.63 | 0.55 |
| S12 | M | 19, 0 | Homozygous: c.[118G>A] + [118G>A] p.[Gly40Ser] + [Gly40Ser] | 0.60 | 0.54 |

The subject codes for the nine RPE65-mutant observers are those used in the gene therapy trial.

temporal contrast sensitivity as a function of frequency at a fixed mean target radiance. This strategy has been adopted before to investigate various pathologies,[25-28] including RP.[29,30]

## METHODS

The data presented here are baseline measurements from a clinical gene therapy trial made in *RPE65*-mutant patients aged between 6- and 23-years old.

The younger patients, aged between 6 and 13 years, who were recruited in the final stages of the trial, could not use the optical testing system used for the older observers. Consequently, we modified the protocol for them and used instead a standard visual display (cathode ray tube, CRT) for testing. We present the results for the two age groups separately in the Results sections. Since this was a clinical protocol, we could not remeasure the older group on the new system. Nevertheless, by using a normal control group, who made measurements on both systems, we have been able to compare the two groups and devise a common model to account for their visual losses.

## Observers

The genetic mutations, sex, age at the time of treatment, and the best-corrected spatial acuity in the left and right eyes of the nine patients are listed in Table 1. The visual acuities were measured using logMAR Early Treatment Diabetic Retinopathy Study charts. Patients judged by clinicians to require "significant" correction were excluded from the clinical trial. The

same subject codes will be used in forthcoming reports of the gene therapy trial.

The older observers (S1, S3, S5, S6, and S12) were measured with stimuli presented in Maxwellian-view and with their heads stabilized using a bite bar, whereas for the younger observers (S7, S8, S10, and S11), stimuli were generated on a CRT with a chin rest to maintain viewing distance and reduce head movements. Observers were instructed to fixate the stimuli foveally. The patients all retained some foveal function, and none of them suffered from severe nystagmus (fixation was not monitored in these experiments, but in other tasks [not described here] their foveal fixation was found to be good but variable. In a comparable group of patients, fixational instabilities of between 0.19° and 0.45° were found.)[31] In terms of the repeatability of these measurements over the 3 years of the measurements, these patients proved to be proficient and reliable psychophysical observers. Repeat measurements of temporal sensitivity made after treatment in the untreated eye (not reported here) were relatively stable.

A group of 10, young, adult volunteers, nine female and one male, and ranging from 21 to 29 years with a mean age of 26.4 years, with normal or corrected to normal visual acuity, provided representative control data. All had normal color vision. The 10 normal volunteers carried out all experimental tasks with both optical systems; we have used their data in comparing the patients' results obtained with different systems. The mean logMAR values for the normal observers with correction was −0.07. Eight observers required no correction during the psychophysical experiments, one wore a corrective lens of −1.0 diopters (D), and another a lens of −4.25 D.

This study conformed to the standards set by the Declaration of Helsinki, and the procedures have been approved by the Moorfields Research Governance Committee, and the local research ethics committee. All subjects or their parents signed informed consent forms

## Maxwellian-View System

**Apparatus.** The Maxwellian-view optical system has been described in full detail elsewhere.[32] Briefly, the optics comprised a standard two-channel system with a 2-mm exit pupil illuminated by a 900-W Xe arc lamp (Osram, Munich, Germany). One channel was used to produce a 4° diameter, circular, 650-nm 'target' field, and the second, to produce a concentric, superimposed circular 480-nm background field of 9° diameter. The wavelengths of the target and background were determined by interference filters (Ealing, South Natick, MA, USA or Oriel, Stratford, CT, USA) inserted into collimated beams in their separate channels. The filters had full bandwidths at half-maximum transmission of between 7 and 11 nm. The radiance in each channel was varied by a combination of neutral-density filters (Oriel), also inserted into the collimated beams, and by the rotation, under computer control, of a circular, variable-neutral-density filter (Rolyn Optics, Covina, CA, USA) located near a focus within the target channel.

Sinusoidal variation of the target radiance was produced by pulse-width modulation of the target beam by a fast, liquid-crystal, light shutter located near a focus in the target beam. The shutter ran at 400 Hz with rise and fall times faster than 50 μs (Displaytech, Longmont, CO, USA), thus producing effectively rectangular pulses at a fixed frequency of 400 Hz but with variable width. The pulse width was varied sinusoidally under computer control using programmable timers (DT2819; Data Translation, Marlborough, MA, USA) to produce sinusoidal stimuli at the desired visible frequencies at modulations up to 92% (frequencies near the 400-Hz rectangular-pulse frequency and above were much too high to be resolved, so that observers saw only the sinusoidally-varying stimuli produced by the variation of the pulse width).

The observer's head was fixed to the system by a hardened dental impression (bite bar) mounted on a milling-machine head that was adjusted to locate the exit pupil of the optics in the center of, and in the plane of the pupil of, the patient's eye. The image of the source in the plane of the observers' pupils was always less than the minimal pupil size so that retinal illumination was not affected by pupil size.

The older patients and all normal controls performed measurements on this system.

**Stimuli.** We measured the temporal properties of vision primarily mediated by long-wavelength sensitive (L-) cones using sinusoidally flickered targets. We refer to the amplitude of the flicker relative to the mean radiance as the "modulation," $m$, which is defined as the conventional Michelson contrast:

$$m = \frac{I_{max} - I_{min}}{I_{max} + I_{min}}, \qquad (1)$$

where $I_{max}$ and $I_{min}$ are the maximum and minimum radiances of the stimulus, respectively. Thus, the sinusoidally flickering stimulus, $A\,(t)$, is given by:

$$A(t) = \bar{R}\{1 + m\,\sin(2\pi f t)\}, \qquad (2)$$

where $\bar{R}$ is the mean radiance and $f$ ( Hz) is the rate of flicker. The modulation, $m$, could be varied under computer control.

*L-cone stimuli.* The 650-nm target wavelength favored detection by cones rather than rods, while the 481-nm background, which delivered 8.24 log quanta s$^{-1}$ deg$^{-2}$ at the

cornea (1.37 log$_{10}$ photopic trolands [td] or 2.53 log$_{10}$ scotopic td), mainly served to suppress the rods, but also selectively desensitized the M-cones at lower target radiances. The background was present for all the experiments reported here. For the cff measurements, the target radiance was varied from 6.5 to 11.5 log$_{10}$ quanta s$^{-1}$ deg$^{-2}$. These target and background conditions isolate the L-cone response over most of the 5 log$_{10}$ unit intensity range, but at high intensities, the M-cones are also likely to contribute to flicker detection. We were largely unconcerned about the possibility of a mixed M- and L-cone response at higher levels. For the modulation sensitivity measurements, the mean target radiance was set to a time-averaged radiance of 10.28 log$_{10}$ quanta s$^{-1}$ deg$^{-2}$ (3.15 log$_{10}$ photopic td).

**Procedures.** The older patients and normal controls light adapted to the background and target for 3 minutes before any measurements and the method of adjustment was used to measure visual responses. They interacted with the computer that controls the apparatus by means of an eight-button keypad, and received information and instructions via tones and a voice synthesizer. Each experiment was repeated three times, usually on separate days. The mean of the results for each experimental run was averaged for each observer separately and the standard error determined. The visual stimulus, focused in the plane of the pupil, was the only visible light source for the observers in an otherwise dark room.

*cff measurements.* The target contrast was held fixed at the maximum value of 92% and the time-average radiance set to values ranging from approximately 6 to 10.7 log$_{10}$ quanta s$^{-1}$ deg$^{-2}$ by the experimenter's inserting neutral-density filters into the target channel. At each target radiance, the observer adjusted the rate of flicker up or down by means of buttons to determine the highest frequency of flicker at which flicker was just visible and indicated satisfaction with their adjustment by pushing a third button. The observer then moved the flicker frequency away from their setting and redetermined their flicker "threshold" twice more before the mean radiance of the target was changed. All three settings and their mean were stored in the computer and the experiment was repeated on three separate occasions for the normal observers and, depending on availability and time constraints, one or two separate occasions for the *RPE65*-mutant observers.

*Temporal contrast-sensitivity measurements (TCSFS).* The mean radiance of both the background and the target were fixed at 10.28 and 8.24 log$_{10}$ quanta s$^{-1}$ deg$^{-2}$, respectively, and the frequency of the flickering target was fixed at values ranging from 0.5 to 50 Hz. The observers adjusted the modulation of the flickering stimulus to determine the lowest contrast at which flicker was just visible (the modulation could be varied up or down in large or small steps depending on the button pressed). The observer determined their modulation threshold three times at any given frequency before the flicker frequency of the target was automatically changed by the computer. Again the average and SEMs obtained on the three different occasions for the normal observers and, depending on availability and time constraints, on two or three separate occasions for the *RPE65*-mutant observers are reported.

**Calibration.** The radiant fluxes of the target and background fields were measured at the plane of the exit pupil using an UDT (United Detector Technology) radiometer, calibrated by the manufacturer (Gamma Scientific, San Diego, CA, USA) against a standard traceable to the US National Bureau of Standards. The neutral-density filters (and circular neutral-density wedge) were calibrated in the optical system, separately for each wavelength used, using the radiometer. The target radiances are reported as time-averaged values. Neutral density filters, fixed and variable, were calibrated in situ for the test and background wavelengths used. A spectroradiometer (EG&G,

San Diego, CA, USA) was used to measure the center wavelength and the bandwidth at one-half the amplitude of each interference filter in situ.

### CRT System

**Apparatus.** Either a calibrated 21" Barco Calibrator (Barco, Kortrijk, Belgium) or a 21" Sony FD Trinitron CRT (Sony, Minato, Japan) were used to display the visual stimuli. The stimuli were generated by a Visual Stimulus Generator (ViSaGe; Cambridge Research Systems Ltd, Rochester, Kent, United Kingdom), which provided intensity resolution of up to 14-bits per gun. The red, green, and blue guns of each monitor were individually gamma-corrected, and thus linearized. The refresh rate of the monitor was set to 160 Hz with a spatial resolution of $800 \times 600$ pixels. A six-key response box was used to collect the observers' responses. The timing of stimulus presentation was implemented by the ViSaGe and was independent of the operating system on the host PC. The younger patients and normal controls performed measurements on this system.

**Stimuli.** The stimuli were chosen to be broadly comparable with those used in the Maxwellian-view system. A flickering 4° diameter "red" circular target was superimposed in the center of a steady, concentric 9° diameter circular "blue" background. The background was generated using only the blue phosphor of the monitor, the spectral distribution of which peaked near 451 nm with a CIE (1931) $x, y$ chromaticity of 0.152, 0.075. The target was generated using only the red phosphor of the monitor, which peaked near 630 nm with an $x, y$ chromaticity of 0.623, 0.342. The maximum luminances of the blue and red primaries depended on the CRT and changed slightly over time, but were between approximately 0.78 and 0.98 $\log_{10}$ cd/m² for the blue phosphor and between approximately 1.20 and 1.40 $\log_{10}$ cd/m² for the red phosphor. Calibrations were carried out daily.

The mean level of the blue background for the cff and TCSF measurements was approximately 0.88 $\log_{10}$ cd/m². The red target for the TCSF measurements had a mean retinal luminance of 0.95 $\log_{10}$ cd/m².

Sinusoidal variation of the target was produced by sampling a sinusoid at appropriate intervals so that, when presented at the frame rate of 160 Hz, sinusoidal flicker at the desired temporal frequency was seen.

**Calibration.** A Radoma spectroradiometer (Gamma Scientific) was used to measure the spectral power distributions of each of the three monitor primaries. A ColorCAL colorimeter (Cambridge Research Systems Ltd.) was used to measure the luminances of each phosphor for gamma correction and to calibrate the experimental conditions daily.

**Procedure.** Procedures were kept as close as possible to those used with the Maxwellian-view system. The major difference was that stimuli were free-viewed monocularly from a distance of 0.5 m (we did not specifically correct for the viewing distance, since the task was temporal not spatial, and used a large target). Also, for the younger observers, the experimenter adjusted either the frequency (for cff measurements) or the modulation (for TCSF measurements) of the target until the observer verbally reported that the flicker percept had just disappeared.

## RESULTS

### L-Cone Critical Flicker Fusion

Figure 1 shows L-cone cff (temporal acuity) data as a function of $\log_{10}$ target radiance for the five adult *RPE65*-mutant observers measured using the Maxwellian-view system. The cff
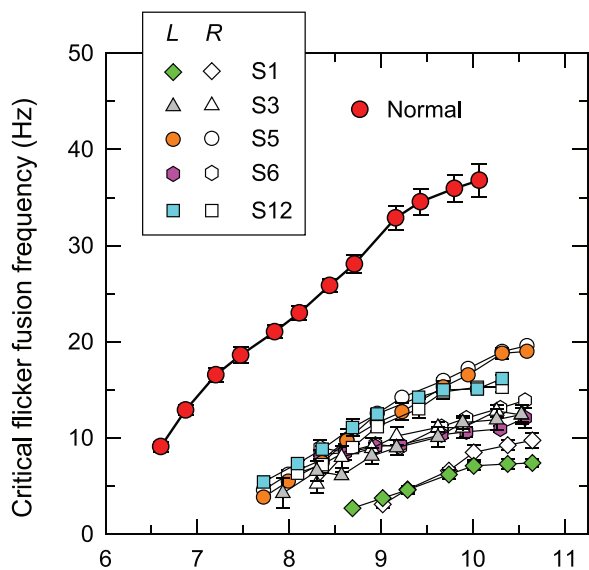
**FIGURE 1.** L-cone critical flicker fusion frequencies (linear scale) measured in Maxwellian-view against a 481-nm background of 8.24 $\log_{10}$ quanta s⁻¹ deg⁻² plotted as a function of the mean log radiance of the 650-nm flickering 4° target. Data are shown for both eyes of the five older observers with the mutant *RPE65* gene, *closed, colored symbols* for the left eye, *open symbols* for the right: S1 (*green* and *open diamonds*), S3 (*gray* and *open triangles*), S5 (*orange* and *open circles*), S6 (*purple* and *open hexagons*), and S12 (*blue* and *open squares*). The mean data for 10 normal observers (*red circles*) are also shown. The *error bars* are ±1 SEM for the *RPE65*-mutant observers, and between observers for the mean data.

(Hz) is plotted against $\log_{10}$ target radiance and the different symbol shapes indicate the results for each observer. Filled colored symbols give results for their left eyes, open symbols for their right eyes. The mean L-cone cff for the normal observers are also plotted (red circles). In this and the next three figures, error bars indicate ±1 SEM within observers for the mutant *RPE65* measurements, and between observers for the normal measurements.

In normal observers, L-cone cff starts to rise at a radiance of approximately 6.5 $\log_{10}$ quanta s⁻¹ deg⁻² and increases steadily until it approaches a plateau above 35 Hz.[33,34] All the observers with the mutant *RPE65* show substantial losses in cff. Flicker is not detected until the mean 650-nm target radiance reaches at least 7.7 $\log_{10}$ quanta s⁻¹ deg⁻², nearly 13 times more intense than for normal observers. Thereafter, the cff increases more slowly with luminance than for the normal observers and approaches much lower limiting cff values.

Notice that for each observer, and for the mean normal observer, there is a radience region over which the cff grows approximately linearly with log intensity. This linear relation is known as the Ferry-Porter law,[35,36] and we shall use the Ferry-Porter "slopes" to characterize the differences among the *RPE65*-mutant observers, and between them and the healthy observers.

Figure 2 shows similar L-cone cff data for both the left and the right eyes of the four younger *RPE65*-mutant observers as a function of $\log_{10}$ target luminance measured using the CRT system. Colored symbols with a central cross give results for their left eyes, open symbols for their right eyes. The mean L-cone cff data for the normal observers measured in the same system are plotted as red squares. The cff (Hz) is again shown
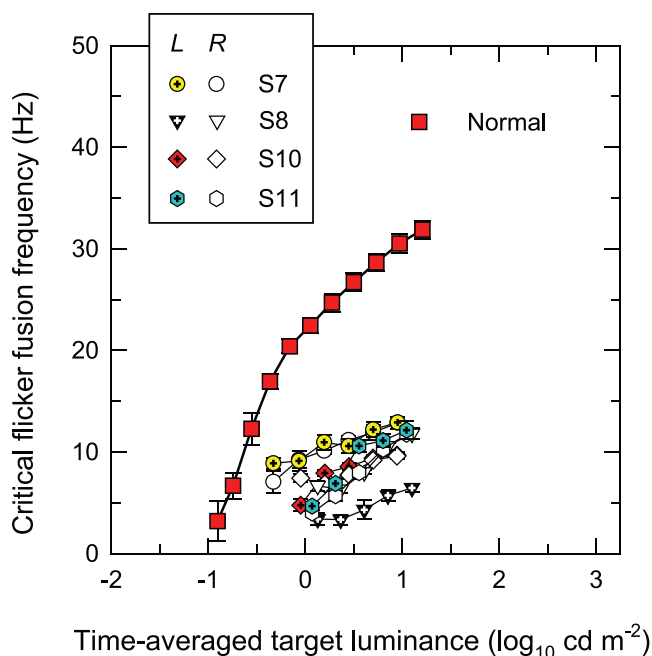
**FIGURE 2.** L-cone critical flicker fusion frequencies measured using a CRT with a blue background of 0.88 $\log_{10}$ cd/m$^2$ plotted as a function of the mean log luminance (cd/m$^2$) of the red target. Data are shown for both eyes of the four younger observers with the mutant *RPE65* measured on the CRT, *crossed, colored symbols* for the left eye, *open symbols* for the right: S7 (*yellow crossed* and *open circles*), S8 (*black crossed* and *open inverted triangles*), S10 (*red crossed* and *open diamonds*), and S11 (*blue crossed* and *open hexagons*). The mean data for the 10 normal observers (*red squares*) are also shown. The *error bars* are ±1 SEM for the *RPE65*-mutant observers, and between observers for the mean data.

on the ordinate but, for the CRT stimuli, intensity is given as luminance ($\log_{10}$ cd/m$^2$).

In normal observers with the CRT system, L-cone cff starts to rise at approximately −1 $\log_{10}$ cd/m$^2$, increases with a gradually decreasing slope reaching approximately 32 Hz at the highest achievable target luminance. As before, the L-cone cff functions for all observers with the mutant *RPE65* show substantial losses in cff. Flicker is not detected until the mean 650-nm target radiance reaches at least −0.5 $\log_{10}$ cd/m$^2$, approximately three times more intense than for normal observers. For the *RPE65*-mutant observers, the function rises only slowly with increasing luminance and rarely exceeds 10 Hz at the highest achievable luminance. As in Figure 1, there is a luminance region for both normal and *RPE65*-mutant observers over which the cff grows approximately linearly with log luminance.

## L-Cone Modulation Sensitivity

Figure 3 shows, in separate panels for each of five older *RPE65*-mutant observers, the logarithm of temporal modulation sensitivity plotted as a function of temporal frequency (logarithmic axis) measured using the Maxwellian-view system. Both right-eye (inverted filled triangles) and left-eye (filled triangles) sensitivities are shown. Also shown in each panel are the mean normal observer modulation sensitivities (red circles). Measurements were made at a time-averaged 650-nm target radiance of 10.28 $\log_{10}$ quanta s$^{-1}$ deg$^{-2}$.

Modulation sensitivity functions that are flat or horizontal at low frequencies but then exhibit an increasing sensitivity loss as the temporal frequency increases are known as "low-pass"

functions, whereas those that also show a sensitivity loss at low frequencies (and therefore appear peaked) are known as "band-pass" functions (the low-frequency loss is usually attributed to surround antagonism[37–42]).

The L-cone modulation sensitivity functions for the mean normal observer are clearly band-pass in shape peaking near 8 Hz[43–45] with sensitivity losses at both high- and low-temporal frequencies. By contrast, the functions for the *RPE65*-mutant observers are roughly similar in shape and, with the exception of S5, are low-pass in shape, but with a substantial variability in overall sensitivity (i.e., in the vertical positions of the functions). At higher frequencies, the L-cone modulation sensitivities for the observers with the mutant *RPE65* fall substantially below the sensitivity of the normal observers.

The logarithmic differences or loss in temporal contrast sensitivity for each of the *RPE65*-mutant observers relative to the mean normal observer are plotted as open symbols in the lower part of each panel. The losses are the logarithmic differences between the data for the *RPE65*-mutant observers and those of the mean normal observer; data for both eyes are shown (the continuous blue lines are model fits to the losses and are described in the Discussion).

Figure 4 shows in separate panels for each of four younger *RPE65*-mutant observers the logarithm of temporal modulation sensitivity measured using the CRT plotted as a function of temporal frequency (logarithmic axis). In each panel, the mean normal observer data are also plotted (red squares). Measurements were made at a time-averaged red phosphor (target) retinal luminance of 0.95 $\log_{10}$ cd/m$^2$ and a blue phosphor (background) retinal luminance of 0.88 $\log_{10}$ cd/m$^2$.

The L-cone modulation sensitivities for the mean normal observer are less band-pass than the measurements obtained with the Maxwellian-view system. This reflects in part the lower luminance levels used with the CRT, but also chromaticity differences, since the phosphors of the CRT have a much broader spectral distribution than the nearly monochromatic lights used in the Maxwellian-view system. Again, the L-cone modulation sensitivities for the observers with mutant *RPE65* fall substantially below the normal observer sensitivities. And again, all are roughly low-pass in shape with very little loss in sensitivity at low frequencies, but with some variability in overall sensitivity.

As in Figure 3, the losses in temporal contrast sensitivity for each of the *RPE65*-mutant observers relative to the mean normal observer are plotted as open symbols in the lower part of each panel. The continuous blue lines are model fits to the losses and will be discussed subsequently.

The losses for the *RPE65*-mutant observers shown as open symbols in Figures 3 and 4 are low-pass in form and consistently show an increasing sensitivity loss as the temporal frequency increases. In each case, the losses are relatively constant at very low frequencies and subsequently fall approximately linearly on these coordinates.

## DISCUSSION

In this section, we concatenate the data from the younger and older observers and also consider their sensitivity losses relative to the normal data to develop common models of the sensitivity losses caused by the *RPE65* mutations. Not only do these models suggest simple underlying mechanisms for the loss, but they can also be used to quantify and compare the severity of the visual losses across different patients. Such models additionally help us to overcome a limitation of this work, which is that for practical reasons, and because of the way the protocol for the clinical trial developed, measurements
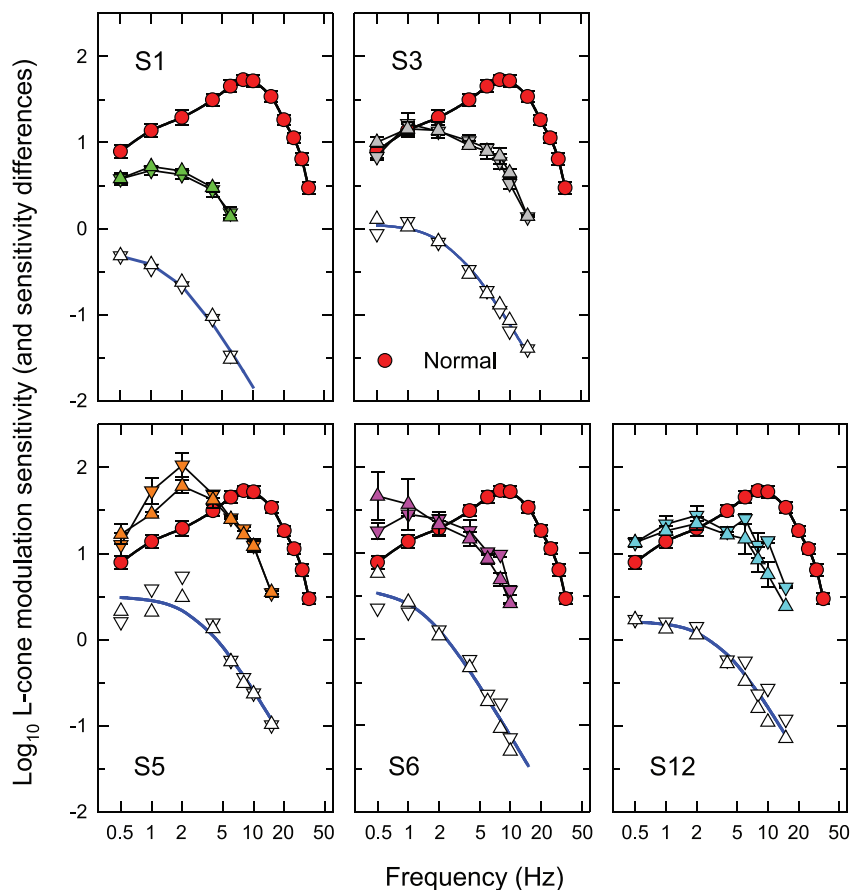
**FIGURE 3.** Each panel shows $\log_{10}$ L-cone modulation sensitivities measured in Maxwellian-view for the left (*filled colored inverted triangles*) and right (*filled colored triangles*) eyes of individual *RPE65*-mutant observers plotted as a function of temporal frequency (Hz, logarithmic axis). The target wavelength was 650 nm with a fixed mean radiance of 10.28 $\log_{10}$ quanta s$^{-1}$ deg$^{-2}$. The target was superimposed on a 480-nm background of 8.24 $\log_{10}$ quanta s$^{-1}$ deg$^{-2}$. The *red circles* repeated in each panel show mean data for the 10 normal observers. In all the panels the *error bars* are ±1 SEM for the *RPE65*-mutant observers, and between observers for the mean data. Also shown in each panel as *open symbols* are the differences in log sensitivity between each affected observer and normal mean. The *blue lines* fitted to the sensitivity differences are model fits described in the Discussion.

in children and older observers were made under different but comparable conditions.

## L-Cone Critical Flicker Fusion

Figure 5 combines all the cff data within a single plot; the cff (Hz, linear scale) is plotted as a function of retinal illuminance (in $\log_{10}$ photopic td). The upper panel of Figure 5 shows the data from normal observers (red circles) and the *RPE65*-mutant observers S1, S3, and S5, S6, and S12 obtained with the Maxwellian-view system all from Figure 1. The intensity measure of Figure 1, log radiance, has been converted to retinal illuminance (log photopic td) using the standard transformation.[46]

The CRT data for the observers with normal vision (red squares) and for S7, S8, S10, and S11 from Figure 2 are also shown on the same axes. The conversion from cd/m$^2$ (Fig. 2) for a 4° target presented on a screen to retinal illuminance in photopic trolands is more complicated. We took the pragmatic approach of using the normal observer cff data measured on the two systems to equate the effective retinal illuminances in the two cases by horizontally shifting the cff data of normal observers measured using the CRT (red squares) to align them with their Maxwellian-view data (red circles; the alignment was made between 20 and 33 Hz, the range over which the cff data plotted on a linear scale as a function of the logarithmic of

luminance are well-described for both sets of normal data by a straight line in accordance with the Ferry-Porter law [the fitted straight blue line in the upper panel]).[35,36] The best-fitting shift from $\log_{10}$ cd/m$^2$ for the normal CRT data to fit the normal Maxwellian-view data plotted in $\log_{10}$ photopic trolands was 0.86 $\log_{10}$ unit. Consequently, the cff data from Figure 2 both for the mean normal observer, and for the *RPE65*-mutant observers, averaged between the eyes, is plotted in Figure 5 after having been shifted by 0.86 $\log_{10}$ unit along the abscissa (error bars for the affected observers have been omitted for clarity).

The data in the middle panel (plotted as in the upper panel at a larger scale but with the same aspect ratio) are the averaged left and right eye data for each affected observer. The blue lines in the middle panel are the best-fitting lines to the linear regions of each *RPE65*-affected observer's data. All fits minimized the sum of the squared deviation between the data and the line. The slopes of the best-fitting lines are tabulated on the left-hand side of Table 2 together with the $R^2$ value for the overall fit. The goodness of fit, indicated by the $R^2$ value of 0.987, is excellent.

The slopes for the *RPE65*-mutant observers range from 1.83 (S6) to 8.04 (S11) Hz per decade with a mean of 4.59. The other parameter in Table 2 is the cff value of the fitted line when the target luminance is 1.5 $\log_{10}$ td (we use this luminance to define the vertical position of the line [rather
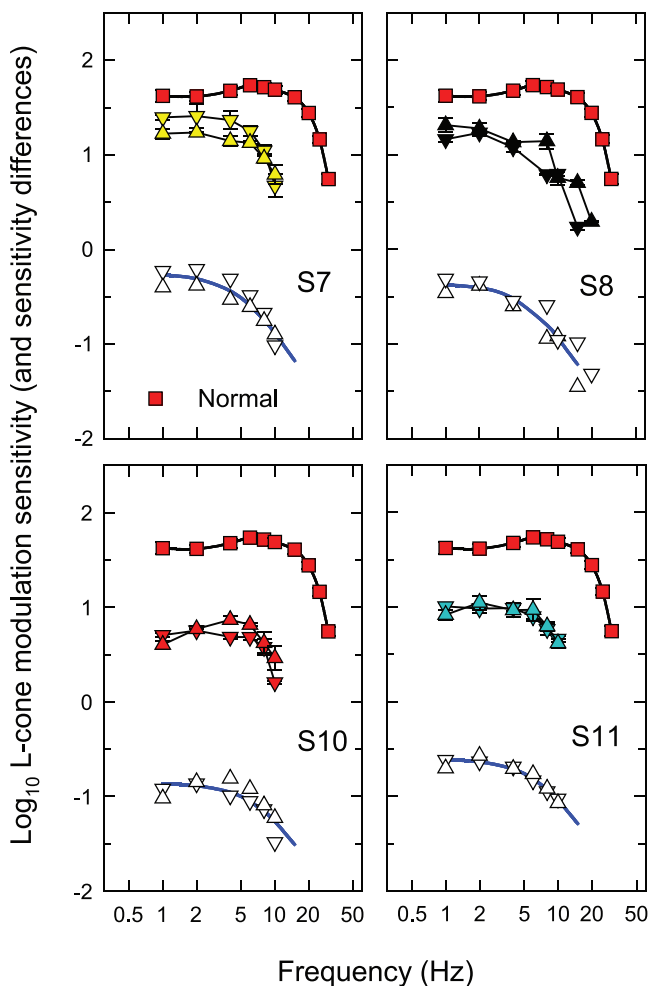
**FIGURE 4.** As for Figure 3 but for four young *RPE65*-mutant observers S7, S8, S10, and S11 measured using the CRT. The mean illuminance of the modulated red target was 0.95 $\log_{10}$ cd/m². The target was superimposed on blue background of 0.88 $\log_{10}$ cd/m². Data for the normal observers using the CRT (*red squares*) are repeated in each panel and the differences in log sensitivity between each *RPE65*-affected observer and the normal are indicated by *open symbols*. Again, the *blue lines* fitted to the sensitivity differences are model fits described in the Discussion.



**FIGURE 5.** The CFF data from Figures 1 and 2 averaged across eyes for each observer and plotted against a common log retinal illuminance scale (photopic td). The symbols for the *RPE65*-affected observers are the same as those for the left eye data plotted in Figures 1 and 2. The *upper panel* also shows the mean data for the 10 normal observers measured in Maxwellian-view (*red circles*) as well as for the *RPE65*-affected observers S1, S3, S5, S6, and S12. The conversion from quanta s⁻¹ deg⁻² (Fig. 1) to photopic trolands was calculated using standard formula. The *upper panel* also shows data for the same 10 normal observers measured with the CRT (*red squares*) and for the four young *RPE65*-affected observers S7, S8, S10, and S11 also measured using the CRT. The conversion for the CRT data from candela per meter squared (Fig. 2) to photopic trolands was based on the horizontal shift of the mean normal data measured with the CRT (*red squares*) required to align with the same observers' mean normal data measured using the Maxwellian view plotted in trolands (*red circles*). The *solid blue line* in the *upper panel* is the Ferry-Porter slope that best fits the aligned normal data. The *middle panel* shows the same data for the *RPE65*-mutant observers plotted at a larger scale and the *solid blue lines* fitted to each data set are the best-fitting Ferry-Porter slopes. (All fitting parameters and slopes can be found in Table 2.) In the *bottom panel*, the CFF data for each observer have been vertically aligned to fit a common 4.53 Hz per decade slope shown as the *solid red line* (see text for further details).

than the more usual intercept at 0 $\log_{10}$ td], since 1.5 $\log_{10}$ td is within the illuminance span of the data). The Ferry-Porter slope for the mean normal observer (blue line, upper panel) is 8.69 Hz per decade with an $R^2$ of 0.993 over the fitted range. The *RPE65* mutation reduces the Ferry-Porter slope by on average approximately 50% compared with the slope for normal observers.

Plotted against the common abscissa in the upper and middle panels of Figure 5, the data obtained using the CRT and Maxwellian-view systems align well. The oldest observer (S1, green diamonds) shows a substantial loss of cff compared with the other observers. The other older observers measured using the Maxwellian-view system (S1, S3, S5, S6, and S12) have slightly lower cffs than the younger observers by on average 1 to 2 Hz consistent with some progressive loss with age.

The cff data for the *RPE65*-mutant observers, like those for the normal observers, are consistent with Ferry-Porter law over a range of approximately 1 or 2 $\log_{10}$ units of illuminance. Consequently, we can use the Ferry-Porter slopes as a means of quantifying and comparing the cff data among the *RPE65*-
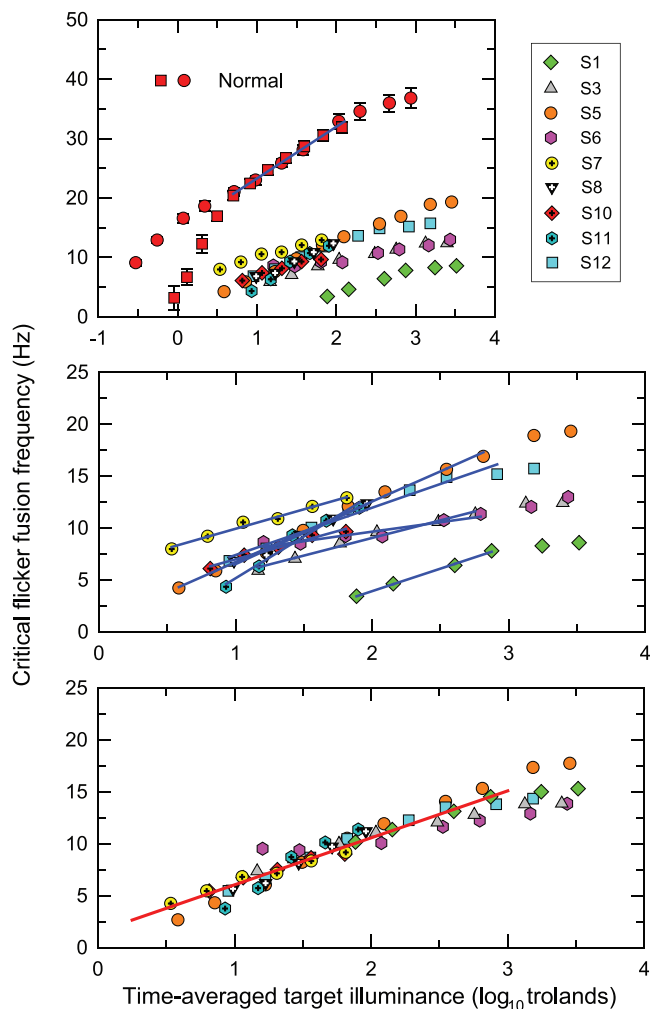
mutant observers and between them and the normal observers.

The Ferry-Porter slopes show little correlation with the sensitivity losses inferred either from the temporal contrast sensitivities ($r^2 = 0.118$) or from the predicted cff values at 1.5 $\log_{10}$ td ($r^2 = 0.012$). Thus, there is little evidence in these data

**TABLE 2.** Critical Flicker Fusion and the Ferry-Porter Law

| Subject | Model 1: Variable Slopes | | | Model 2: Common Slope | | |
|---|---|---|---|---|---|---|
| | cff at 1.5 $\log_{10}$ td | Slopes | $R^2$ | cff at 1.5 $\log_{10}$ td | Slopes | $R^2$ |
| S1 | $1.74 \pm 1.32$ | $4.34 \pm 0.55$ | 0.987 | $1.58 \pm 0.77$ | $4.53 \pm 0.25$ | 0.916 |
| S3 | $7.34 \pm 0.62$ | $3.39 \pm 0.31$ | | $6.84 \pm 0.63$ | | |
| S5 | $9.63 \pm 0.37$ | $5.82 \pm 0.20$ | | $9.86 \pm 0.54$ | | |
| S6 | $8.72 \pm 0.63$ | $1.83 \pm 0.31$ | | $7.43 \pm 0.63$ | | |
| S7 | $11.79 \pm 0.49$ | $3.75 \pm 0.39$ | | $12.04 \pm 0.49$ | | |
| S8 | $9.51 \pm 0.82$ | $5.99 \pm 0.54$ | | $9.47 \pm 0.57$ | | |
| S10 | $8.80 \pm 0.73$ | $3.64 \pm 0.53$ | | $9.56 \pm 0.54$ | | |
| S11 | $9.17 \pm 0.79$ | $8.04 \pm 0.54$ | | $8.88 \pm 0.56$ | | |
| S12 | $9.67 \pm 0.48$ | $4.56 \pm 0.24$ | | $9.68 \pm 0.60$ | | |
| Mean | $8.49 \pm 0.93$ | $4.59 \pm 0.60$ | – | $8.30 \pm 0.98$ | 4.53 | – |

Columns 2 and 3 in the left-hand section give the parameters and standard errors of the best-fitting Ferry-Porter lines to each observers' data when the slope of the line was allowed to vary across observers: column 2 gives the vertical position (in Hz) of the best fitting lines that correspond to a target illuminance of 1.5 log td, column 3 gives the slope of the best-fitting lines in Hz per decade. The $R^2$ value for the overall fit of model 1 was 0.987 (mean values and values for the mean normal data are shown at the bottom). The right hand section shows the vertical positions in Hz of the best fitting lines that correspond to a target illuminance of 1.5 log td when the data are fit using a common slope of 4.53 Hz per decade. The goodness-of-fit measure, $R^2$, was 0.916.

for the slopes becoming shallower as the sensitivity loss progresses.

Most of the Ferry-Porter slope estimates for the *RPE65*-mutant observers (left-hand side of Table 2) differ from the mean slope of 4.59 Hz per decade by less than 1.4 Hz per decade. This suggests that a useful way of quantifying and summarizing the relative losses for the *RPE65*-mutant observers is to fix the Ferry-Porter line slope at a common best-fitting slope for all the *RPE65*-affected observers and then to determine the best-fitting vertical shifts of that line required to align it with each set of cff data. The fits were done simultaneously and the results given in the right-hand panel of Table 2. The lower panel of Figure 5 shows the best-fitting Ferry-Porter line (red solid line), which has a slope of 4.53 Hz per decade, together with the data for each observer vertically shifted to align with the red-solid line. As can be seen in the panel, and by the $R^2$ measure of goodness-of-fit measure of 0.916 on the right in Table 2, the Ferry-Porter slope provides a very plausible description of the aligned RPE65 data.

The best-fitting vertical shifts are also tabulated in right-hand side of Table 2 in terms of the cff values of the fitted line at 1.5 $\log_{10}$ td. Not unexpectedly, given that the cff and temporal contrast sensitivities at higher frequencies are linked, there is a moderate correlation ($r^2 = 0.55$) between this measure of sensitivity loss and the measure based on the temporal contrast sensitivity.

What can we learn from the Ferry-Porter law slopes? The slopes can be compared with the high-frequency slope of temporal contrast-sensitivity functions (plotted as log contrast-sensitivity versus *linear* frequency) simply by rotating the cff versus log radiance plot clockwise by 90°. The shallower Ferry-Porter slopes in Hz per decade in the *RPE65*-mutant observers implies that they suffer much steeper losses in contrast sensitivity with increasing frequency than normal observers, as we indeed find. Such changes are consistent with the damage or loss caused by the *RPE65*-mutation resulting in a much more sluggish visual response.

## L-Cone Modulation Sensitivity

Our approach to understanding and modelling the sensitivity losses shown in Figures 3 and 4 is to take the conventional approach of assuming that the visual process can be treated as a cascade of leaky integrating stages (or buffered RC circuits), the outputs of which decay exponentially after exposure to a brief pulse of light. An exponential decay with a time constant of $\tau$ can, by a simple Fourier transform, be converted into an amplitude versus frequency function, the magnitude of the Fourier transform of exponential decay. The amplitude, $A(f)$, of $n$ cascaded, identical, leaky integrators as a function of frequency, $f$, is given by:

$$A(f) = \tau^n \left[ (2\pi f \tau)^2 + 1 \right]^{-\frac{n}{2}}, \quad (3)$$

where $\tau$ is the time constant in seconds, assumed to be common to all stages, and $n$ is the number of stages. In the model, light adaptation shortens the time constants of some of the stages and so speeds up the visual response allowing more rapid flicker to be seen. This approach of modelling the eye as a linear temporal filter has a long tradition.[42,45,47–50] In terms of phototransduction, the approach can be compared with considering the system as a cascade of independent reactions each having first-order exponential decays. In the leaky integrator, the response to a pulse decays exponentially with time; while in the reaction, the concentration of the reactant decays exponentially with time.[51]

By modelling the sensitivity differences between the affected and normal observers, we are effectively discounting stages of the cascade with the same time constants in both normal and *RPE65*-mutant observers as well as any other processes they may have in common. We then assume that the remaining differences reflect changes in the time constants of stages that the observers share, and/or that the mutation produces additional limiting stages in the affected eyes. We model the losses for the *RPE65*-mutant observers by assuming that they effectively have more stages than the normal observer.

We varied the number of additional stages, $n$, in preliminary fits; and found that we could simplify the model by assuming that each affected observer has two additional stages (i.e., $n = 2$ in Equation 3). In general, when the data were simultaneously modelled and $n$ was allowed to vary, $n = 2$ was the closest integer. Put more formally, the fitting equation (with $n = 2$) was:

$$\log_{10}[A_N(f)/A_A(f)] = -\log_{10}\left[ \tau^2 \left[ (2\pi f \tau_A)^2 + 1 \right]^{-1} \right] + k, \quad (4)$$

**TABLE 3.** Two-Stage Low-Pass Filter Models With Variable Time Constants

| Subjects | Shifts, $k$ | $\tau$ (Corner Frequency) | $R^2$ |
|---|---|---|---|
| S1 | $-0.85 \pm 0.06$ | $94.47 \pm 11.88$ (1.68) | 0.959 |
| S3 | $-0.10 \pm 0.04$ | $58.96 \pm 5.41$ (2.70) | |
| S5 | $0.42 \pm 0.04$ | $54.10 \pm 4.96$ (2.94) | |
| S6 | $-0.13 \pm 0.04$ | $112.53 \pm 12.12$ (1.41) | |
| S7 | $0.21 \pm 0.08$ | $28.68 \pm 3.95$ (5.55) | |
| S8 | $0.19 \pm 0.07$ | $26.25 \pm 3.07$ (6.06) | |
| S10 | $-0.06 \pm 0.11$ | $19.67 \pm 3.44$ (8.09) | |
| S11 | $0.14 \pm 0.11$ | $20.71 \pm 3.45$ (7.69) | |
| S12 | $0.24 \pm 0.05$ | $47.76 \pm 4.39$ (3.33) | |
| Mean | $0.00 \pm 0.12$ | $51.46 \pm 11.03$ ($4.38 \pm 0.84$) | |

Columns 2 and 3 give the parameters and standard errors of the best-fitting two-stage filter model to the corrected modulation sensitivity losses for each *RPE65*-mutant observer: column 2 gives the vertical logarithmic shift of the filter to fit each data set relative to the mean shift, column 3 the time constant in milliseconds and, in brackets, the corresponding corner frequency in Hz. The goodness-of-fit measure for the overall fit, $R^2$, was 0.959.

where the subscripts $N$ and $A$ indicate parameters of the frequency responses of the normal and affected observer, respectively. The value of $k$ represents a frequency independent change in overall sensitivity (a shift on logarithmic ordinates) and $\tau$ represents the time constant common to both stages. Equation 4 was simultaneously fitted to the whole *RPE65*-mutant dataset to find the best-fitting values of $k$ and $\tau$ for each affected observer. These values along with their standard errors are tabulated in Table 3. The model fits, shown by the continuous blue lines in Figures 3 and 4, are good with an $R^2$ goodness-of-fit of 0.959.

One concern, however, is that the contrast sensitivity differences measured in Maxwellian-view (for S1, S3, S5, S6, and S12) begin to fall at lower temporal frequencies than those measured with the CRT (for S7, S8, S10, and S11). The reason for the differences can be found in the normal observer's contrast-sensitivity data measured with the two systems. If the normal contrast-sensitivity data obtained with the CRT are vertically aligned with the Maxwellian-view data at higher frequencies, the two sets of normal contrast sensitivity data agree well at 6 Hz and above. At lower frequencies, the Maxwellian-view data show greater low-frequency attenuation (up to 0.49 $\log_{10}$ unit at 1 Hz). The differences in the mean normal observers' log sensitivity are plotted as a function of frequency in the upper panel of Figure 6 (black circles).

The differences across measuring systems at low frequencies are almost certainly due to the different stimulus conditions. In the Maxwellian-view system, the mean luminance of the background is 1/60th of the target, which means that the modulated sinusoidal 650-nm flicker is effectively monochromatic. By contrast, the luminance of the background produced by the blue CRT phosphor is only 7/10th of the target produced by the red CRT phosphor, which means that the modulated CRT flicker will have a strong chromatic component and it is well known that chromatic flicker is less subject to low-frequency attenuation than monochromatic flicker[52–54] as we find.

The differences in low-frequency attenuation found for normal observers between the two systems, and attributable to the different display systems, will affect the *estimates* of sensitivity loss for the *RPE65* observers as well. To correct for these differences, we adjusted the RPE65 sensitivity losses estimated with the Maxwellian-view system by removing the additional low-frequency attenuation from the normal
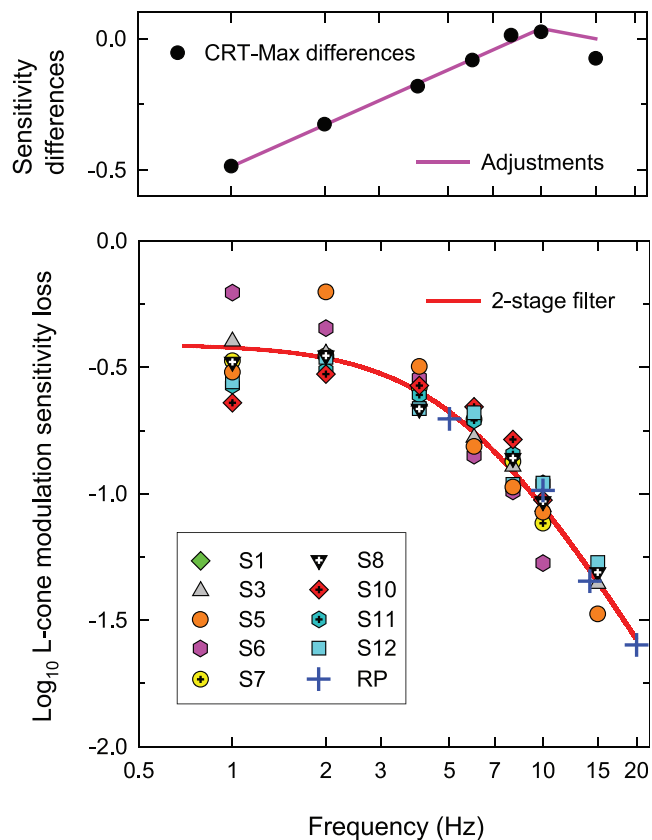


**FIGURE 6.** The *upper panel* shows the mean log sensitivity differences between results from the Maxwellian-view and CRT systems for the 10 normal observers as a function of frequency (Hz, logarithmic scale). The *purple solid line* shows the adjustment made to correct for the differences attributable to differences in the visual display systems. The *lower panel* shows the log sensitivity loss for the *RPE65*-affected observers relative to the normal sensitivity as a function of frequency (Hz, logarithmic scale). For clarity, the individual *RPE65*-mutant data have been averaged across eyes and shifted vertically to align with the common filter. The symbols for the *RPE65*-affected observers are the same as those used in Figure 5. The *solid red line* shows the prediction for the two-stage low-pass filter that best fits the sensitivity losses for all *RPE65*-mutant observers (see text for further details). The set of loss data shown as *blue crosses* and labelled "RP" are replotted from Figure 5B of Tyler et al.,[30] and are the left eye data for the "multiplex" RP observer with the greatest loss; they have been shifted vertically by 0.24 log unit to align with the data and the two-stage filter model.

observer data according to the linear function shown by the solid purple line plotted in the upper panel of Figure 6. After the adjustments, shown in the lower panel of Figure 6, the sensitivity losses for the two groups are more consistent, so that we could proceed with modelling the data.

We can simplify the model by assuming common time constants for the two-stage filter across all affected observers, and then characterize the relative losses in terms of the best-fitting vertical shift of the filter required to align the sets of modulation sensitivity losses the mean loss. The lower panel of Figure 6 shows the best-fitting common two-stage filter (red solid line), both stages of which have the common time constant of 29.45 ms (The additional data points from Tyler et al.[30] [blue crosses], and the blue line will be discussed later.) The best-fitting vertical logarithmic shifts of the filter to align the data sets with the mean and the best-fitting common time constants are tabulated in Table 4. The goodness-of-fit measure, $R^2$, was 0.898.

**TABLE 4.** Two-Stage Low-Pass Filter Model With Common Time Constants for All Observers

| Subjects | Shifts, $k$ | $\tau$ (Corner Frequency) | $R^2$ |
|---|---|---|---|
| S1 | −0.61 ± 0.05 | 29.45 ± 1.42 (5.40) | 0.898 |
| S3 | −0.04 ± 0.04 | | |
| S5 | 0.50 ± 0.04 | | |
| S6 | 0.09 ± 0.04 | | |
| S7 | 0.16 ± 0.04 | | |
| S8 | 0.09 ± 0.04 | | |
| S10 | −0.32 ± 0.04 | | |
| S11 | −0.09 ± 0.04 | | |
| S12 | 0.23 ± 0.04 | | |
| Mean | 0.00 ± 0.11 | | |

Columns 2 and 3 give the parameters and standard errors of the best-fitting two-stage filter model to the adjusted modulation sensitivity losses for each *RPE65*-mutant observer: column 2 gives the vertical logarithmic shift of the common filter to fit each data set relative to the mean shift, column 3 the time constant in milliseconds and, in brackets, the corner frequency in hertz of the common filter. The goodness-of-fit measure for the overall fit, $R^2$, was 0.898.

The lower panel of Figure 6 shows the sensitivity losses for the *RPE65*-affected observers after they have been vertically aligned with the prediction of the best-fitting two-stage filter. As can be seen, the common two-stage filter provides a reasonable description and simplification of the aligned *RPE65*-mutant data. The vertical shifts required to align each set of losses with the best-fitting filter provide another estimate of the overall sensitivity losses for each observer. These agree well with the estimates of sensitivity loss obtained from aligning the cff data along a common Ferry-Porter slope (Table 2, column 5).

We speculate that the two-stage filter added to the *RPE65*-mutant visual pathway in our model can be linked to changes at the molecular or neural level caused directly or indirectly by the mutation. At the molecular level, the additional filters might be linked to a limiting sluggish molecular process (with comparable time-constants to the model values) that maintains residual function within damaged photoreceptors. Alternatively, they might be linked to changes at the neural level. For example, substantial photoreceptor loss in the affected observers could cause the predominant and most effective cone signals to come from the sluggish, spatially-extensive surrounds of spatially-opponent neurons instead of from their centers as in normal observers, with the extra surround sluggishness being characterized by the additional filters in the model. Rather than being a passive process, the photoreceptor loss might instead trigger an active rewiring and reorganization[55,56] that produces a novel postreceptoral organization not found in normal retinae (but one that is consistent with the addition of two additional low-pass filters).

As noted above, measurements of cff and temporal contrast sensitivity have been made before in RP observers, but RP observers of unknown genotype. For example, the cff measurements by Tyler et al.[30] on nine "simplex" RP observers (sufferers from families in which only one sufferer is affected over three generations) were found to have a Ferry-Porter slope comparable with that of normal observers; this is clearly inconsistent with our cff results for our LCA2 observers. However, Tyler et al.[30] also made contrast-sensitivity measurements in four "multiplex" observers (sufferers from families in which only siblings from the same generation are affected over three generations). Of these, the two least sensitive RP observers have temporal modulation-sensitivity losses comparable with the losses we find for LCA2 observers. We have replotted the left eye data for their most insensitive observer

(see their Fig. 5B) as crosses in the lower panel of Figure 6. As can be seen, the losses for this observer are consistent not only with the losses for the LCA2 observers but also with the two-stage model.

Felius and Swanson[29] found changes in temporal sensitivity but little change in the shapes of foveal temporal contrast-sensitivity functions for their 18 RP observers. However, by selecting observers with spatial acuities better than or equal to 20/32 and with no visual field defects within 6° of the fovea, they effectively excluded observers with LCA2.

In summary, *RPE65*-mutant observers show consistent and characteristic losses of temporal acuity (cff) and temporal contrast sensitivity. The Ferry-Porter slopes for the *RPE65*-mutant observers range from 1.83 to 8.04 Hz per decade of luminance with a mean of 4.59 compared with a mean slope of 8.69 ± 0.23 Hz per decade of luminance in normal observers. Fitting a common Ferry-Porter slope to all *RPE65*-mutant observers suggests an approximately 50% reduction in the Ferry-Porter slope from 8.69 Hz per decade of luminance in normal observers to 4.53 Hz per. The losses in temporal contrast-sensitivity relative to normal observers can be characterized by the interposition of two identical, sluggish low-pass filters. Fitting a common two-stage filter to all *RPE65*-mutant observers suggests the interposition of a two-stage filter with a common time constant of 29.45 ms.

## References

1. Perrault I, Rozet JM, Gerber S, et al. Leber congenital amaurosis. *Mol Genet Metabol*. 1999;68:200–208.

2. Hanein S, Perrault I, Gerber S, et al. Leber congenital amaurosis: comprehensive survey of the genetic heterogeneity, refinement of the clinical definition, and genotype-phenotype correlations as a strategy for molecular diagnosis. *Hum Mut*. 2004;23:306–317.

3. Gu SM, Thompson DA, Srikumari CR, et al. Mutations in *RPE65* cause autosomal recessive childhood-onset severe retinal dystrophy. *Nat Genet*. 1997;17:194–197.

4. Perrault I, Rozet JM, Ghazi I, et al. Different functional outcome of retGC1 and RPE65 gene mutations in Leber congenital amaurosis. *Am J Hum Genet*. 1999;64:1225–1228.

5. Marlhens F, Bareil C, Griffoin JM, et al. Mutations in *RPE65* cause Leber's congenital amaurosis. *Nat Genet*. 1997;17:139–141.

6. Lotery AJ, Namperumalsamy P, Jacobson SG, et al. Mutation analysis of 3 genes in patients with Leber congenital amaurosis. *Arch Ophthalmol*. 2000;118:538–543.

7. Thompson DA, Gyurus P, Fleischer LL, et al. Genetics and phenotypes of *RPE65* mutations in inherited retinal degeneration. *Invest Ophthalmol Vis Sci*. 2000;41:4293–4299.

8. Stone EM. Leber Congenital Amaurosis–a model for efficient genetic testing of heterogeneous disorders: LXIV Edward Jackson memorial lecture. *Am J Ophthalmol*. 2007;144:791–811.

9. Morimura H, Fishman GA, Grover SA, Fulton AB, Berson EL, Dryja TP. Mutations in the *RPE65* gene in patients with autosomal recessive retinitis pigmentosa or Leber congenital amaurosis. *Proc Natl Acad Sci U S A*. 1998;95:3088–3093.

10. Schatz P, Preising M, Lorenz B, Sander B, Larsen M, Rosenberg T. Fundus albipunctatus associated with compound heterozygous mutations in *RPE65*. *Ophthalmology*. 2011;118:888–894.

11. Bowne SJ, Humphries MM, Sullivan LS, et al. A dominant mutation in *RPE65* identified by whole-exome sequencing causes retinitis pigmentosa with choroidal involvement. *Eur J Hum Genet*. 2011;19:1074–1081.

12. Redmond TM, Yu S, Lee E, et al. *Rpe65* is necessary for production of 11-*cis*-vitamin A in the retinal visual cycle. *Nat Genet*. 1998;20:344–351.

13. Mata NL, Moghrabi WN, Lee JS, et al. Rpe65 is a retinyl ester binding protein that presents insoluble substrate to the isomerase in retinal pigment epithelial cells. *J Biol Chem*. 2004;279:635–643.

14. Thompson DA, Gal A. Genetic defects in vitamin A metabolism of the retinal pigment epithelium. *Dev Ophthalmol*. 2003;37:141–154.

15. Lamb TD, Pugh EN Jr. Dark adaptation and the retinoid cycle of vision. *Progr Retin Eye Res*. 2004;23:307–380.

16. Jin M, Li S, Moghrabi WN, Sun H, Travis GH. Rpe65 is the retinoid isomerase in bovine retinal pigment epithelium. *Cell*. 2005;122:449–459.

17. Moiseyev G, Chen Y, Takahashi Y, Wu BX, Ma JX. RPE65 is the isomerohydrolase in the retinoid visual cycle. *Proc Natl Acad Sci U S A*. 2005;102:12413–12418.

18. Redmond TM, Poliakov E, Yu S, Tsai JY, Lu Z, Gentleman S. Mutation of key residues of RPE65 abolishes its enzymatic role as isomerohydrolase in the visual cycle. *Proc Natl Acad Sci U S A*. 2005;102:13658–13663.

19. Lamb TD. Photopigments and the biophysics of transduction in cone photoreceptors. In: Gegenfurtner K, Sharpe LT, eds. *Color Vision: From Genes to Perception*. Cambridge, UK: Cambridge University Press; 1999:89–101.

20. Burns ME, Baylor DA. Activation, deactivation and adaptation in vertebrate photoreceptor cells. *Annu Rev Neurosci*. 2001;24:779–805.

21. Znoiko SL, Crouch RK, Moiseyev G, Ma JX. Identification of the RPE65 protein in mammalian cone photoreceptors. *Invest Ophthalmol Vis Sci*. 2002;43:1604–1609.

22. Wu BX, Moiseyev G, Chen Y, Rohrer B, Crouch RK, Ma JX. Identification of RDH10, an all-trans retinol dehydrogenase, in retinal Müller cells. *Invest Ophthalmol Vis Sci*. 2004;45:3857–3862.

23. Berger W, Kloeckener-Gruissem B, Neidhardt J. The molecular basis of human retinal and vitreoretinal diseases. *Progr Retin Eye Res*. 2010;29:335–375.

24. Daiger SP, Sullivan LS, Bowne SJ. Genes and mutations causing retinitis pigmentosa. *Clin Genet*. 2013;84:132–141.

25. Simonson E, Brožek J. Flicker fusion frequency: background and applications. *Physiol Rev*. 1952;32:349–378.

26. Kayazawa F, Yamamoto T, Itoi M. Temporal-modulation transfer-function in patients with retinal diseases. *Ophthalmic Res*. 1982;14:409–415.

27. Stockman A, Smithson HE, Michaelides M, Moore AT, Webster AR, Sharpe LT. Residual cone vision without α-transducin. *J Vis*. 2007;7(8)1–13.

28. Stockman A, Smithson HE, Webster AR, et al. The loss of the PDE6 deactivating enzyme, RGS9, results in precocious light adaptation at low light levels. *J Vis*. 2008;8(10)11–10.

29. Felius J, Swanson WH. Photopic temporal processing in retinitis pigmentosa. *Invest Ophthalmol Vis Sci*. 1999;40:2932–2944.

30. Tyler CW, Ernst W, Lyness AL. Photopic flicker sensitivity losses in simplex and multiplex retinitis pigmentosa. *Invest Ophthalmol Vis Sci*. 1984;25:1035–1042.

31. Jacobson SG, Aleman TS, Cideciyan AV, et al. Human cone photoreceptor dependence on RPE65 isomerase. *Proc Natl Acad Sci U S A*. 2007;104:15123–15128.

32. Stockman A, Plummer DJ, Montag ED. Spectrally-opponent inputs to the human luminance pathway: slow +M and -L cone inputs revealed by intense long-wavelength adaptation. *J Physiol*. 2005;566:61–76.

33. Hecht S, Verrijp CD. The influence of intensity, color and retinal location on the fusion frequency of intermittent illumination. *Proc Natl Acad Sci U S A*. 1933;19:522–535.

34. Hecht S, Shlaer S. Intermittent stimulation by light. V. The relation between intensity and critical frequency for different parts of the spectrum. *J Gen Physiol*. 1936;19:965–977.

35. Ferry ES. Persistence of vision. *Am J Sci*. 1892;44:192–207.

36. Porter TC. Contributions to the study of flicker. Paper II. *Proceedings of the Royal Society of London Series A*. 1902;70:313–329.

37. Schober HAW, Hilz R. Contrast sensitivity of the human eye for square-wave gratings. *J Opt Soc Am*. 1965;55:1086–1091.

38. Robson JG. Spatial and temporal contrast sensitivity functions of the visual system. *J Opt Soc Am*. 1966;56:1141–1142.

39. Nachmias J. Effect of exposure duration on visual contrast sensitivity with square-wave gratings. *J Opt Soc Am*. 1967;57:421–427.

40. Ratliff F, Knight BW, Toyoda J-I, Hartline HK. Enhancement of flicker by lateral inhibition. *Science*. 1967;158:392–393.

41. Kelly DH. Flickering patterns and lateral inhibition. *J Opt Soc Am*. 1969;59:1361–1370.

42. Watson AB. Temporal sensitivity. In: Boff K, Kaufman L, Thomas J, eds. *Handbook of Perception and Human Performance*. New York, NY: Wiley; 1986:6.1–6.43.

43. de Lange H. Research into the dynamic nature of the human fovea-cortex systems with intermittent and modulated light. I. Attenuation characteristics with white and colored light. *J Opt Soc Am*. 1958;48:777–784.

44. Kelly DH. Visual responses to time-dependent stimuli I. Amplitude sensitivity measurements. *J Opt Soc Am*. 1961;51:422–429.

45. Roufs JAJ. Dynamic properties of vision. II. Theoretical relationship between flicker and flash thresholds. *Vision Res*. 1972;12:279–292.

46. Wyszecki G, Stiles WS. *Color Science: Concepts and Methods, Quantitative Data and Formulae. 2nd ed*. New York: Wiley; 1982.

47. Ives HE. A theory of intermittent vision. *J Opt Soc Am*. 1922;6:343–361.

48. de Lange H. Experiments on flicker and some calculations on an electrical analogue of the foveal systems. *Physica*. 1952;18:935–950.

49. Kelly DH. Visual responses to time-dependent stimuli II. Single-channel model of the photopic visual system. *J Opt Soc Am*. 1961;51:747–754.

50. Levinson J, Harmon LD. Studies with artificial neurons. III. Mechanisms of flicker-fusion. *Kybernetik*. 1961;1:107–117.

51. Connors KA. *Chemical Kinetic: The Study of Reaction Rates in Solution*. New York: VCH; 1990.

52. Kelly DH. Luminous and chromatic flickering patterns have opposite effects. *Science*. 1975;188:371–372.

53. Kelly DH, van Norren D. Two-band model of heterochromatic flicker. *J Opt Soc Am*. 1977;67:1081–1091.

54. Varner D, Jameson D, Hurvich LM. Temporal sensitivities related to color theory. *J Opt Soc Am A*. 1984;1:474–481.

55. Jones BW, Watt CB, Frederick JM, et al. Retinal remodeling triggered by photoreceptor degenerations. *J Comp Neurol*. 2003;464:1–16.

56. Marc RE, Jones BW, Watt CB, Strettoi E. Neural remodeling in retinal degeneration. *Progr Retin Eye Res*. 2003;22:607–655.